



Air-oxidation of a Co-based amorphous ribbon at 400–600 °C

W. Kai^{a,*}, P.C. Lin^a, W.S. Chen^a, P.C. Kao^a, R.T. Huang^a, P.K. Liaw^b

^a Institute of Materials Engineering, National Taiwan Ocean University, Keelung, 20224, Taiwan, ROC

^b Department of Materials Science and Engineering, The University of Tennessee, Knoxville, TN 37996-2200, USA

ARTICLE INFO

Article history:

Received 2 July 2010

Received in revised form 8 December 2010

Accepted 8 December 2010

Available online 15 December 2010

Keywords:

Oxidation

Co₆₉B₁₂Si₁₂Fe₄Mo₂Ni₁ amorphous ribbon

CoO

ABSTRACT

The oxidation behavior of a commercial Co₆₉B₁₂Si₁₂Fe₄Mo₂Ni₁ amorphous ribbon (Co6-AR) was studied over the temperature range of 400–600 °C in dry air. The results showed that virtually no oxidation occurred at 400 °C. On the other hand, the oxidation kinetics of the Co6-AR alloy at 450–600 °C generally followed a multi-stage parabolic-rate law, and the parabolic-rate constants (k_p values) tend to increase with increasing temperature. It was found that the oxidation rates of the glassy alloy are slower than those of pure Co, indicative of a better oxidation resistance. An exclusive scale of CoO was observed after the oxidation of the glassy alloy in the temperature range of interest, and several crystalline phases formed on the substrate beneath the scale, consisting of pure Co (both FCC and HCP structures), Co₃B, Co₂Si, CoFe, and Co₂B (absent at 450 °C), which indicated the occurrence of crystallization.

© 2010 Elsevier B.V. All rights reserved.

1. Introduction

Iron- and cobalt-based amorphous alloys have been intensively studied since the past two decades because of their unique magnetic and mechanical properties as well as chemical stability [1–4]. A typical result shown in the literature is to have an ultra-high fracture strength of 5185 MPa for a Co₄₃Fe₂₀Ta_{5.5}B_{31.5} amorphous alloy [4]. Furthermore, particular examples of interest are to use them for the soft magnet-tube and micro-electronic core applications [5,6]. Besides, it may be also important to understand their thermal-activated degradation in oxidizing atmospheres when using those alloys at elevated temperatures in ambient environments. In spite of numerous data reported in the literature on the mechanical and magnetic behaviors of Co-based amorphous alloys, their oxidation behavior was still lack of study.

Most recently, a series of Co–Fe–Ni–Si–B–M amorphous systems (where M=Mo, Cr, Al) were developed, and the results showed that most of the alloys possess excellent thermal and mechanical properties [7,8]. For example, a commercial product of Co₆₉B₁₂Si₁₂Fe₄Mo₂Ni₁ glassy ribbon, as named Metglass-2705, had been reported to exhibit a higher Curie temperature (T_c) and crystallization temperature (T_x) around 365 and 520 °C, respectively. In addition, this glassy ribbon also exhibited a good magnetic induction value (I_s) of 0.7 T [8,9]. Furthermore, this amorphous alloy contained significant amounts of common alloying elements (Co, B, and Si), which could offer a lower material-cost to meet the needs

for practical applications in industries. In order to apply the Co6-AR at elevated temperatures in industrial applications, it is essential to understand its oxidation properties. Thus, the aim of this study is to investigate the air-oxidation behavior of the Co6-AR at elevated temperatures. The oxidation of pure Co is also explored in the same environments for comparative purposes.

2. Experimental

The Co6-AR sheets of 25 mm × 25 mm (20 μm thick) were directly purchased from the manufacturer in USA, while pure-Co sheets (99.99% pure) of 30 mm × 30 mm × 20 mm were obtained from the local supplier in Taiwan. Typical XRD spectra of the Co6-AR are shown in Fig. 1a, revealing that a wide-broadening peak near $2\theta = 45.60^\circ$ was noted, indicative of the amorphous structure of the glassy ribbon. Both Co6-AR and pure Co samples were initially cut into about 3 mm × 3 mm sheets, polished and ground with 1-μm diamond paste, cleaned with acetone and methanol, and immediately dried before the tests.

The thermal stability of the Co6-AR samples was done by the differential scanning calorimetry (DSC) at a heating rate of 20 °C/min. As shown in Fig. 1b, DSC results showed that the glass transition temperature (T_g) and crystallization temperature (T_x) were around 481.8 and 523.9 °C, respectively. Thus, the present T_x result is close to that in the literature mentioned above. Oxidation tests and characterization of the substrate and scales were similar to those described previously [10], except for that the heating and cooling rates of the TGA furnace were set at 20 °C/min.

3. Results and discussion

3.1. Oxidation kinetics

Parabolic plots of the oxidation kinetics of the Co6-AR and pure Co over the temperature range of 400–600 °C in dry air are shown in Fig. 2. As can be seen in this figure, nearly no mass-gain data can be recorded by TGA at 400 °C, which implied that virtually no

* Corresponding author.

E-mail address: wkai@mail.ntou.edu.tw (W. Kai).

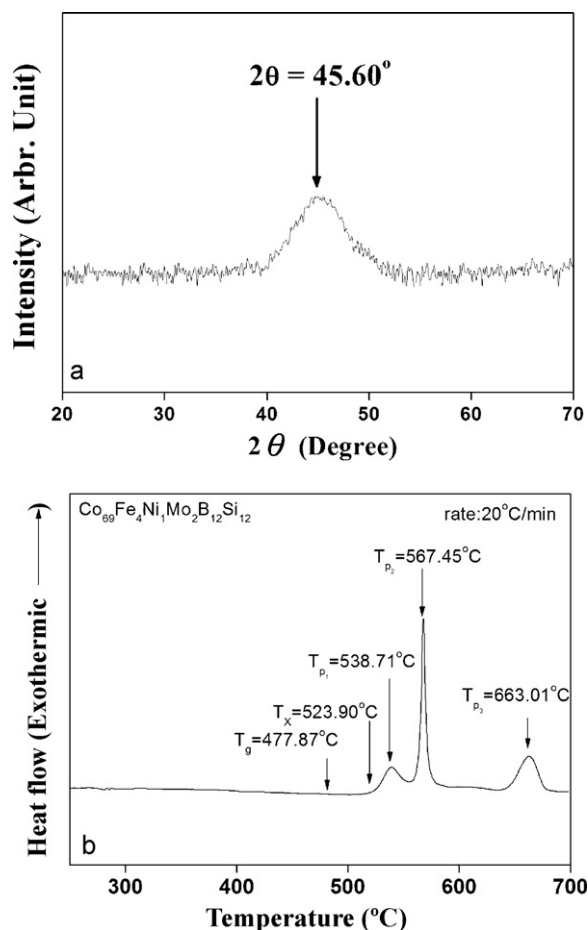


Fig. 1. (a) XRD spectra and (b) DSC curves of the as-received Co6-AR.

oxidation occurred at this temperature. At higher temperatures ($T \geq 450^\circ\text{C}$), the oxidation kinetics of the glassy alloy generally followed a two-stage parabolic-rate law, with its oxidation-rate constants (k_p values) increasing steadily with temperature. This observation further indicates that diffusion is the rate-controlling step for the scaling behavior of the Co6-AR during oxidation. The measured k_p values of the Co6-AR and pure Co are tabulated in Table 1. As can be seen in the table, the k_p values of the Co6-AR are lower than those of pure Co by factors of 22.6, 54.8, and 10.3 at 450, 500, and 600 °C, respectively. The lower k_p values measured for the Co6-AR further indicated that this amorphous ribbon exhibited a better oxidation resistance than pure Co. In addition, the observed discrepancy of the k_p values for the Co6-AR with respect to pure Co may be due to the formation of various scales and crystalline phases, as discussed later.

3.2. Scale constitution and phases

A typical SEM micrograph of the surface of Co6-AR after a 48-h exposure at 400 °C is shown in Fig. 3a, revealing that numerous

Table 1
Air-oxidation rate constants of pure Co and the Co-based amorphous ribbon at 450–600 °C.

Material	Temperature		
	450 °C	500 °C	600 °C
Pure Co	2.53×10^{-13}	7.24×10^{-12}	2.09×10^{-11}
Co6-AR	1.12×10^{-14}	1.32×10^{-13}	2.02×10^{-12}

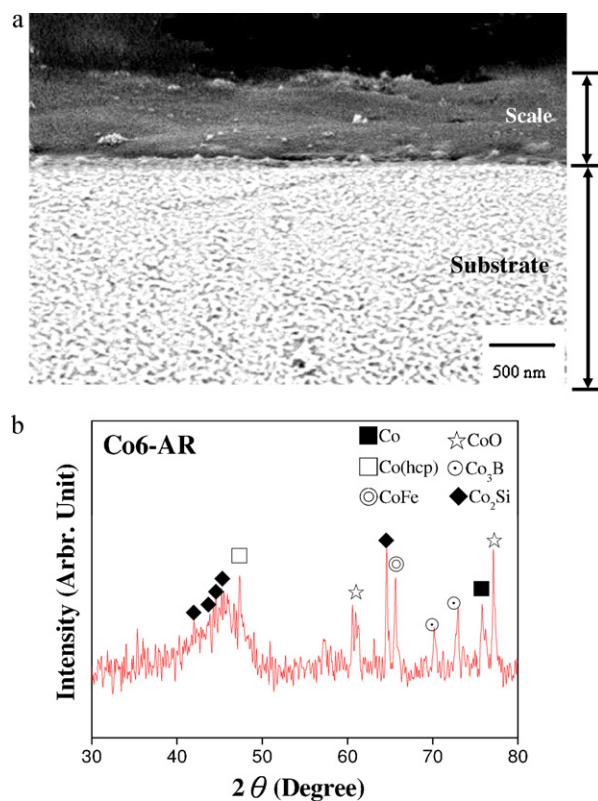


Fig. 2. Parabolic plots of the oxidation kinetics of (a) the Co-based amorphous ribbon at 400–600 °C and (b) pure Co at 450–600 °C in dry air.

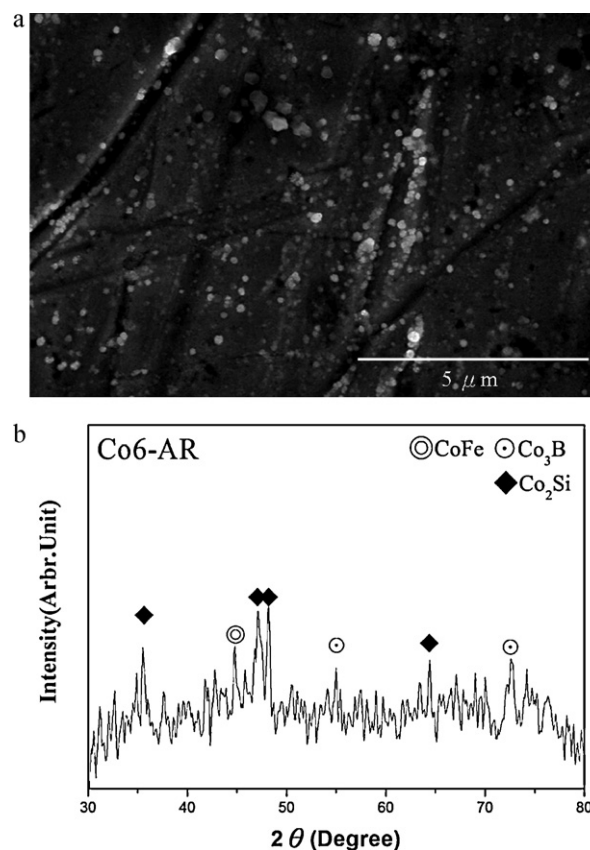


Fig. 3. (a) SEM topograph and (b) corresponding XRD spectra of the Co6-AR alloy after oxidation for 48 h at 400 °C.

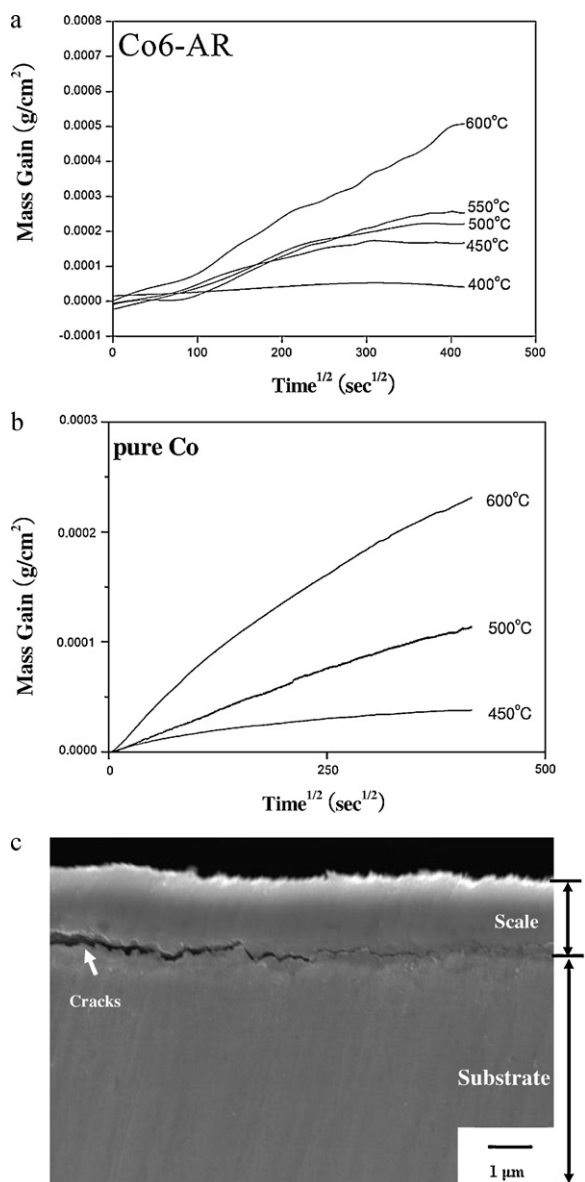


Fig. 4. (a) Cross-sectional BEI micrograph and (b) corresponding XRD analyses of the Co-based amorphous ribbon (c) Cross-sectional BEI micrograph of pure Co oxidized at 450 °C for 48 h.

tiny precipitates were observed. EDS analyses of four different precipitates gave the average composition (in at.%) of Co(78.08%), Si(15.20%), Fe(4.74%), and Mo(1.98%). However, since the light element of B was unable to detect, the exact composition of crystalline phases is further analyzed by XRD spectra, as shown in Fig. 3b. At least three crystalline phases were obtained, consisting of mostly Co₂Si and minor amounts of Co₃B and CoFe. Thus, it is clearly that no evidence of any oxide was detected on the Co6-AR after oxidation for 48 h at 400 °C. A cross-sectional backscattered-electron-image (BEI) micrograph of the Co6-AR oxidized at 450 °C for 36 h is shown in Fig. 4a, revealing a thin scale layer. The XRD analyses (Fig. 4b) revealed that the scale consisted of a thin CoO layer intermixed with un-corroded pure Co (both FCC and HCP structures), Co₃B, CoFe, and Co₂Si. For comparison, a BEI micrograph of the scales formed on pure Co after the same temperature and exposure duration is shown in Fig. 4c. Although not shown here, XRD analyses indicated that the scales formed on pure Co consisted of CoO and Co₃O₄. It should be pointed out that the scale thickness formed on the Co6-AR is much thinner (around 655 ± 45 nm) than that formed on pure

Co (1.27 ± 0.11 μm), which is in good agreement with the observed slow oxidation rate for the amorphous ribbon. Interestingly, the crystallization to form both FCC- and HCP-Co modifications after oxidation is observed because the hexagonal structure is relatively stable at room temperature for pure cobalt. Very likely, the oxidation of the amorphous ribbon resulted in the local change of the initial composition, which may depart from the ideal case for pure cobalt. In addition, the presence of two modifications of pure Co and three intermetallics may be due to the thin-scale nature, which allows the X-ray penetration down to the non-oxidized Co6-AR substrate. Nevertheless, the formation of the crystalline phases further indicated that the phase transformation for the glassy substrate was taken place although the oxidation temperature is much lower than T_g (481.8 °C). It is also noted that at least two different images were present in the Co6-AR substrate after SEM operation with BEI mode, indicative of the formation of multiple crystalline phases. However, EDS analyses failed to identify their exact composition because their average grain size is too small to beyond the SEM resolution limits.

Typical BEI micrographs and the corresponding XRD analyses of the cross-sections of the Co6-AR oxidized at 500–600 °C for 36 h are further shown in Fig. 5, revealing a single-layer scale. The total thickness of the scales is much thicker than that at 450 °C, being about 1.18 ± 0.30 μm at 500 °C and 1.60 ± 0.25 μm at 600 °C under the same exposure time. Based on XRD analyses, the scale is also composed exclusively of CoO, which intermixed with the non-oxidized crystalline phases of Co, Co₃B, Co₂B, CoFe, and Co₂Si.

The additional presence of Co₂B at 500 °C or higher temperatures is unexpected, which deserved further TEM analyses. A typical TEM bright-field image and SAD patterns of the cross-sectional scale and substrate are shown in Fig. 6. Numerous nano-sized particles presented in the substrate beneath the scales (Fig. 6a), and SAD analyses taken from a dark region showed that both Co₃B and Co₂B were co-existed as ring patterns, which further confirms the formation of Co₂B. Another TEM bright-field image taken from the innermost scale (Fig. 6b) showed a continuous oxide layer, whose SAD spot-patterns under a zone axis of [0 1 1] confirmed the formation CoO. No evidence of Co₃O₄ and other oxides was detected by TEM analyses, which was further in good agreement with XRD analyses.

An interesting aspect to further discuss is to possibly form other oxides in oxidation of Co6-AR since it contained high amounts of B and Si. According to the Gibbs free energies of formation (ΔG_f° ; in unit of kJ/mol O₂) of possible oxides at 450 °C [11], the values of ΔG_f° for both SiO₂ (−779.2) and B₂O₃ (−720.2) are much more negative than those of CoO (−365.8) and Co₃O₄ (−315.6). One would expect that the formation of either SiO₂, B₂O₃, or both should be thermodynamically favorable, because their dissociation partial pressures are much lower than the local oxygen pressure between the substrate and CoO. However, none of them was observed by XRD, EPMA, and TEM analyses. It is most likely that the scaling rate of CoO is much faster than that of other oxides, so that the formation of SiO₂ or B₂O₃ becomes unfavorable.

On the other hands, one would also expect that the activities of B and Si in the substrate should be relatively increased when a certain amount of Co was preferentially oxidized, which in turn resulted in an increase the possibility to form intermetallic Co₃B, Co₂B and Co₂Si precipitates, as observed above. Perhaps, the formation of these intermetallics in the substrate could further provided a partly blocking effect to reduce the availability of Co in the substrate, which in turned subsequently reduced its outer diffusion for the metal-oxygen reaction, thereby leading the reduction of oxidation rates of the amorphous ribbon.

Another interesting aspect to further discuss is the possible reasons for the slow oxidation rate with respect to that of pure Co. Unlike the formation of a duplex layer of CoO and Co₃O₄ on pure

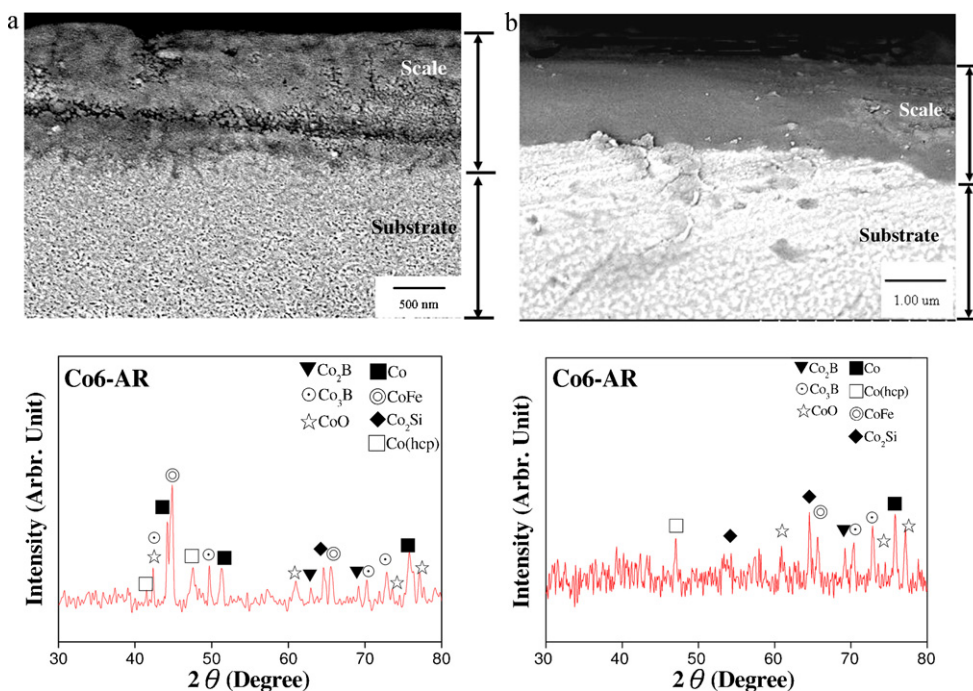


Fig. 5. Cross-sectional BEI micrographs and corresponding XRD analyses of the Co6-AR oxidized for 48 h (a) at 500 °C and (b) at 600 °C.

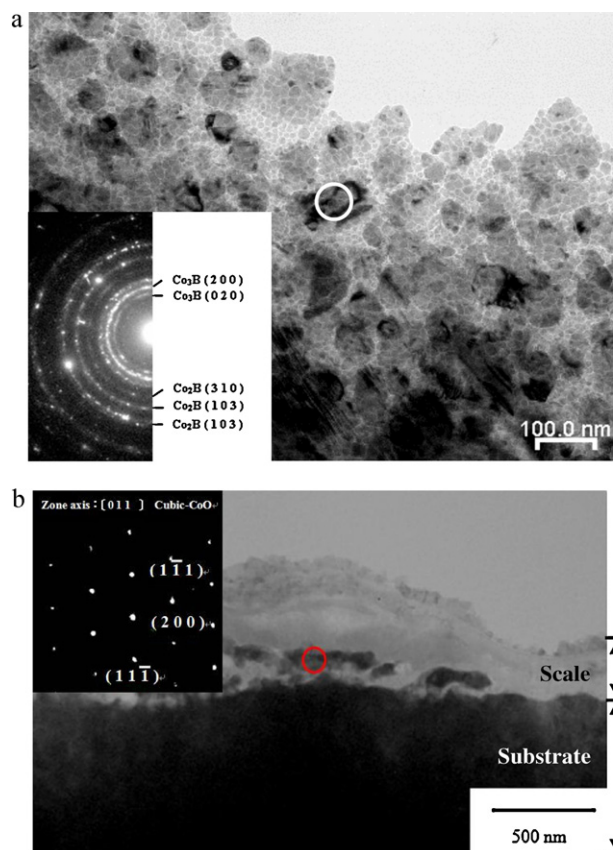


Fig. 6. (a) TEM bright-field micrograph and SAD ring-patterns of the Co6-AR substrate and (b) TEM bright-field micrograph and SAD spot-patterns of the scale formed on the Co6-AR oxidized at 500 °C for 96 h.

Co at 450–600 °C, a single scale-layer of CoO formed on the Co6-AR. In a review of the defect chemistry, Co_{1-x}O was a metal-deficient, P-type conducting oxide with its non-stoichiometry values (x) being around 0.01 at 1150 °C and 1 atm O_2 [12]. Conversely, Co_3O_4 was an n-type conducting oxide at higher partial pressures of oxygen ($P_{\text{O}_2} \geq 2.1 \times 10^4$ Pa) and at 900 °C although its non-stoichiometry values were not given [12]. It is very likely that the defect species at 450–600 °C may retain unchanged, so that the scaling rates of complex scales of double cobalt oxides of CoO and Co_3O_4 on pure Co would be much faster than that of the single CoO layer on the Co6-AR. Thus, it may conclude that the formation of an exclusive CoO layer is responsible for the slower oxidation rate of the Co6-AR as compared to the fast-growth of CoO and Co_3O_4 for pure Co.

3.3. Short-term oxidation

In order to study the relationship between the initial oxidation and crystallization of the Co6-AR, short-term oxidation tests were

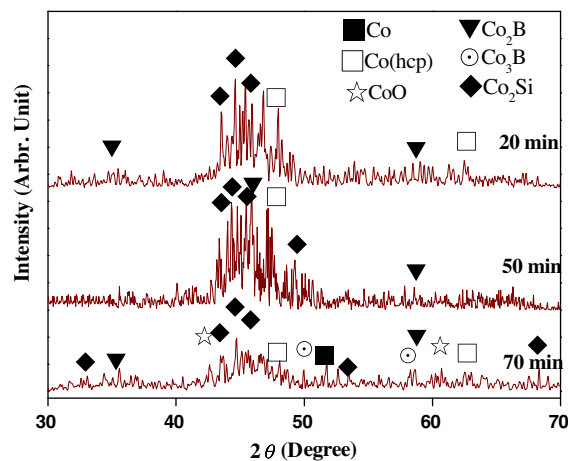


Fig. 7. XRD analyses of the crystalline phases formed on the Co-based amorphous ribbon oxidized at 500 °C for various durations of time.

performed at 500 °C with various durations of time. Typical XRD analyses of the amorphous alloy after the oxidation at various durations of 500 °C are shown in Fig. 7. As can be seen in this figure, three crystalline phases of pure Co (both FCC and HCP structures) and Co₂Si formed on the amorphous substrate after an initial oxidation for 20 min, which further implies that the Co6-AR undergoes the preferential crystallization before any oxidation of the substrate. In addition, the fourth crystalline phase of Co₃B was also detected after a 50-min exposure, while the CoO phase further formed after a prolong exposure (up to 70 min) at the same temperature. Thus, the scaling behavior for the Co6-AR at 500 °C is the first formation of the four crystalline phases, and followed by the growth of CoO at the later exposure.

4. Conclusions

The oxidation behavior of a Co₆₉B₁₂Si₁₂Fe₄Mo₂Ni₁ amorphous ribbon (Co6-AR) over the temperature range of 400–600 °C was characterized. Several conclusions can be made.

1. The oxidation kinetics of the Co6-AR followed a two-stage parabolic-rate law with their rate constants increasing with temperature.
2. No evidence of any oxide was detected on the Co6-AR after oxidation for 48 h at 400 °C although XRD spectra revealed three crystalline phases of mostly Co₂Si and minor amounts of Co₃B and CoFe.
3. The Co6-AR exhibited a better oxidation resistance than pure Co, having its k_p values were lower than those of pure Co by factors of 10.3–54.8 from 450 °C to 600 °C.
4. The scales formed on the Co6-AR consisted of an exclusive layer of CoO, while the scales formed on pure Co consisted of CoO and Co₃O₄. At least five various non-oxidized crystalline

phases formed on the substrate beneath the scale, consisting of pure Co (both FCC and HCP structures), Co₃B, Co₂Si, and CoFe, indicative of the crystallization of the amorphous substrate during the oxidation over the temperature range of interest.

Acknowledgments

Partly financial support by the National Science Council of Republic of China under the Grant nos. of NSC-97-E-2218-110-010 and NSC 98-E-2218-110-007 is greatly acknowledged. TGA equipment support by the National Taiwan Ocean University under the Grant no. of NTOU-RD972-04-03-01-01 is also appreciated. Special thanks are indebted to Mr. C.T. Wu and Z.Z. Liang in the Department of System Engineering and Science, National Tsing Hua University for their technical supports of TEM.

References

- [1] A. Inoue, *Acta Mater.* 48 (2000) 279.
- [2] M. Hagiwara, A. Inoue, T. Masumoto, *Mater. Sci. Eng.* 54 (1982) 197–207.
- [3] Y. Gan, *J. Non-Cryst. Solids* 291 (2001) 199.
- [4] A. Inoue, B.L. Shen, H. Koshiba, H. Kato, A.R. Yavari, *Acta Mater.* 52 (2004) 1631–1637.
- [5] C.G. Kim, K.J. Jang, D.Y. Kim, S.S. Yoon, *Appl. Phys. Lett.* 75 (1999) 2114.
- [6] D. Raybould, K.S. Tan, *J. Mater. Sci.* 20 (1982) 2776–2786.
- [7] R. Germano, G. Ausiano, V. Iannotti, L. Lanotte, C. Luponio, *Sens. Actuators* 81 (2000) 134.
- [8] Y. Iwami, Y. Okazaki, A. Saito, *J. Magn. Magn. Mater.* 254–255 (2003) 127–129.
- [9] G. Bordin, G. Buttion, A. Cecchetti, M. Cecchetti, M. Poppi, *J. Magn. Magn. Mater.* 153 (1996) 285–292.
- [10] W. Kai, I.F. Ren, P.C. Kao, R.T. Huang, C.T. Liu, *Intermetallics* 17 (2009) 205–210.
- [11] I. Barin, *Thermochemical Data for Pure Substance*, 3rd edn., American Chemical Society and American Institute of Physics for National Bureau of Standards, Weinheim, New York, 1995.
- [12] P. Kofstad, *High Temperature Corrosion*, Elsevier Applied Science, London and New York, 1988.